Journal of Power Sources 196 (2011) 6144–6152

Contents lists available at ScienceDirect

Journal of Power Sources

journal homepage: www.elsevier.com/locate/jpowsour

Systematic studies on benzimidazole derivatives: Molecular structures and their hydrogen bond networks formation toward proton transfer efficiency

Autchara Pangon[a], Puripong Totsatitpaisan[a], Priew Eiamlamai[a], Kimiko Hasegawa[b], Mikio Yamasaki[b], Kohji Tashiro[c,*], Suwabun Chirachanchai[a,d,**]

[a] The Petroleum and Petrochemical College, Chulalongkorn University, Soi Chula 12, Phyathai Road, Pathumwan, Bangkok 10330, Thailand
[b] X-ray Research Center, Rigaku Corporation, Akishima, Tokyo 196-8666, Japan
[c] Department of Future Industry-Oriented Basic Science and Materials, Graduate School of Engineering, Toyota Technological Institute, Hisakata 2-12-1, Tempaku, Nagoya 468-8511, Japan
[d] Center for Petroleum and Petrochemicals, and Advanced Materials, Chulalongkorn University, Bangkok 10330, Thailand

ARTICLE INFO

Article history:
Received 8 December 2010
Received in revised form 19 February 2011
Accepted 25 February 2011
Available online 23 March 2011

Keywords:
Benzimidazole
Hydrogen bond network
Polymer electrolyte membrane
Proton transfer
Packing structure
Fuel cell

ABSTRACT

A series of benzimidazole derivatives with varied benzimidazole groups, i.e., mono- (**B-1**), di- (**B-2** and **B-3**), and trifunctional (**B-4**), are focused as model compounds for a systematic study to understand the relationship between the hydrogen bond network including its consequent packing structure and the proton conductivity in an anhydrous system. The different number of benzimidazole units in a molecule initiates a different packing structure under the hydrogen bond network of which **B-1** provides a perpendicular hydrogen bond network, **B-2** and **B-3** provide a parallel hydrogen bond network under a lamellar structure, and **B-4** forms a helical hydrogen bond network under a columnar structure. The study reveals that the proton conductivity of heterocycles in anhydrous system and doped with polyphosphoric acid is significant when (i) more benzimidazole groups is exist in a single molecule to form hydrogen bond networks, (ii) each benzimidazole is closely packed to allow an effective proton transfer from an NH in one benzimidazole unit to another, and (iii) the packing structure forms a specific channel to favour efficient proton transfer such as columnar packing structure. The present work is a guideline to develop high efficient benzimidazole-based membrane for a high temperature polymer electrolyte membrane fuel cell (PEMFC).

1. Introduction

Sulfonated-perfluorinated polymer electrolyte membrane, in particular Nafion®, is one of the most practical materials for PEMFC because of its significant proton transfer efficiency [1–4]. Since the membrane needs hydration, its conductivity dramatically decreases when the operating temperature is close to the boiling point of water [5–7]. The fact that intermediate temperature range (100–150 °C) helps in improving reaction kinetics, decreasing CO tolerance and enhancing proton conductivity [8,9], the anhydrous membrane for PEMFC system becomes an important point for development.

Heterocycles, such as imidazole, benzimidazole and pyrazole, are known for their proton hopping through the protonation of nitrogen atom and the structural re-orientation under a hydrogen bond network [10]. Therefore, heterocycles are a possible alternative material for membranes functioning in the intermediate operating temperature range [10–13]. Bozkurt et al. [14] developed anhydrous membranes of polyacrylic acid/imidazole polymer electrolyte and the conductivity increased with the number of imidazoles per polymer repeat unit. Yamada and Honma [15] showed that a high-ordered structured composite based on two-dimensional proton-conducting pathways of acidic surfactant of monododecyl phosphate and a basic surfactant of 2-undecylimidzole gave a proton conductivity as high as 10^{-3} S cm^{-1} at 150 °C. The proton conductivities at elevated temperature of other heterocyclic molecules were variously reported, for example, a blend of 1-methylimidazole and poly(vinylphosphoric acid) [16], azole derivatives in Nafion® composite membranes [12].

Although there are many reports of heterocycles containing polymers as polymer electrolyte membranes (PEMs), most are related to investigations of the material properties and their conductivity while the key point to achieve proton transfer with

* Co-corresponding author at: Graduate School of Engineering, Toyota Technological Institute, Hisakata 2-12-1, Tempaku, Nagoya 468-8511, Japan. Tel.: +81 0 52 809 1790; fax: +81 0 52 809 1793.
** Corresponding author at: The Petroleum and Petrochemical College, Chulalongkorn University, Soi Chula 12, Phyathai Road, Pathumwan, Bangkok 10330, Thailand. Tel.: +66 2 218 4134; fax: +66 2 215 4459.
E-mail addresses: ktashiro@toyota-ti.ac.jp (K. Tashiro), csuwabun@chula.ac.th (S. Chirachanchai).

0378-7753/$ – see front matter © 2011 Elsevier B.V. All rights reserved.
doi:10.1016/j.jpowsour.2011.02.093

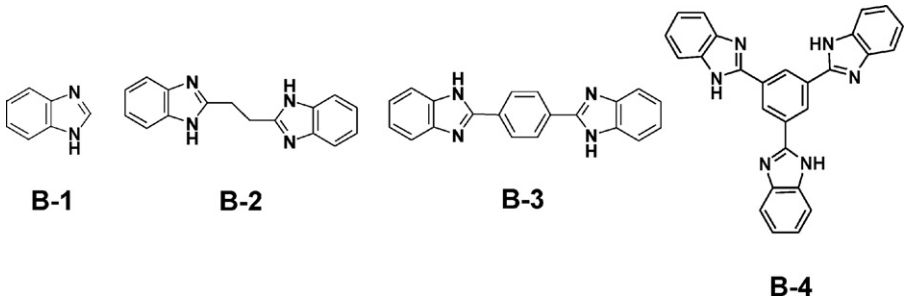

Scheme 1. Chemical structure of model compounds: benzimidazole (**B-1**), ethylene-1,2-di-2-benzimidazole (**B-2**), 1,4-bis(2-benzimidazolyl)benzene (**B-3**) and 1,3,5-tri(2-benzimidazolyl)benzene (**B-4**).

high-efficiency is still not clear. Based on this viewpoint, it can be mentioned that an understanding of the relationship between the hydrogen bond networks of the heterocycles together with their consequent packing structures and the proton conductivity should lead to a fundamental development of heterocycles with an effective proton transfer property. In order to obtain this information, it is important to consider a systematic study of the heterocyclic molecules. Here, benzimidazole (**B-1**) as monofunctional, ethylene-1,2-di-2-benzimidazole (**B-2**) and 1,4-bis(2-benzimidazolyl)benzene (**B-3**) as difunctional, and 1,3,5-tri(2-benzimidazolyl)benzene (**B-4**) as trifunctional derivatives (Scheme 1) are considered as model compounds. The work focuses on the hydrogen bond network and the molecular packing structures and also extends to an investigation of proton conductivity to establish the relationship between the molecular structure and the proton transfer efficiency.

2. Experimental

2.1. Materials

All chemicals were reagent grade and were used without further purification. Benzimidazole (**B-1**), 1,3,5-benzenetricarbonyltrichloride, 1,2-phenylenediamine, polyphosphoric acid (PPA), and deuterated dimethyl sulfoxide (DMSO-d_6) were purchased from Aldrich, Germany. Succinyl chloride was purchased from Fluka, Switzerland. Terephthaoyl chloride was the product of Wako, Japan. Sodium hydroxide, *p*-xylene, and methanol were obtained from Carlo Erba, Italy. DMSO, ethylene glycol, and *N*-methylpyrrolidone (NMP) were obtained from Labscan, Ireland. Glass filters, GC-50, were bought from Advantec, Japan.

2.2. Synthesis of the benzimidazole model compounds *B-2*, *B-3*, and *B-4*

Benzimidazole derivatives **B-2**, **B-3**, and **B-4** were synthesized as model compounds as in the previous reports [17–19]. In brief, terephthaloyl chloride (6.6×10^{-2} mmol mL^{-1}) was dissolved in *p*-xylene and added dropwise into a vigorously stirred solution containing an excess of 1,2-phenylenediamine (7.9×10^{-1} mmol mL^{-1}) under a nitrogen atmosphere at 80 °C for 24 h. The precipitates were collected and neutralized with 1.0 M NaOH solution in methanol. The crude products were further refluxed in NMP at 150 °C under vacuum for 24 h to allow the cyclization to obtain **B-3**. Similarly, **B-2** and **B-4** were prepared but using succinyl chloride (5.6×10^{-2} mmol mL^{-1}) and 1,3,5-benzenetricarbonyltrichloride (8.7×10^{-3} mmol mL^{-1}), respectively.

2.2.1. Ethylene-1,2-di-2-benzimidazole, *B-2*

Yield 64%. FTIR (KBr, ν cm^{-1}) 1622 (w), 1590 (w), 1542 (w), 1453 (s), 1276 (s), 748 (s). ^{1}H NMR (δ ppm, 500 MHz, DMSO-d_6, 298 K): 12.31 (2H, s, N*H*), 7.53 (2H, d, $^2J_{HH}$ = 7.30 Hz, Ar*H*), 7.43 (2H, d, $^2J_{HH}$ = 7.50 Hz, Ar*H*), 7.15–7.10 (4H, m, Ar*H*), 3.38 (4H, s, CH_2). MS calcd for $C_{16}H_{14}N_4$ *m*/*z* 262.12, found 263.13. Anal. Calcd. for $C_{16}H_{14}N_4$: C, 73.28; H, 5.34; N, 21.37. Found: C, 71.99; H, 5.70; N, 20.49.

2.2.2. 1,4-Bis(2-benzimidazolyl)benzene, *B-3*

Yield 59%. FTIR (KBr, ν cm^{-1}) 1622 (w), 1586 (w), 1570 (w), 1453 (s), 1279 (w), 738 (s). ^{1}H NMR (δ ppm, 500 MHz, DMSO-d_6, 298 K): 13.03 (2H, s, N*H*), 8.36 (4H, s, Ar*H*), 7.71 (2H, d, $^2J_{HH}$ = 7.70 Hz, Ar*H*), 7.57 (2H, d, $^2J_{HH}$ = 7.50 Hz, Ar*H*), 7.28–7.23 (4H, m, Ar*H*). MS calcd for $C_{20}H_{14}N_4$ *m*/*z* 310.12, found 310.64. Anal. Calcd. for $C_{20}H_{14}N_4$: C, 77.40; H, 4.55; N, 18.05. Found: C, 77.74; H, 4.26; N, 17.90.

2.2.3. 1,3,5-Tri(2-benzimidazolyl)benzene, *B-4*

Yield 69%. FTIR (KBr, ν cm^{-1}) 1623 (w), 1593 (w), 1536 (w), 1462 (w), 1278 (s), 740 (s). ^{1}H NMR (δ ppm, 500 MHz, DMSO-d_6, 298 K): 13.37 (3H, s, N*H*), 9.12 (3H, s, Ar*H*), 7.77 (3H, d, $^2J_{HH}$ = 7.65 Hz, Ar*H*), 7.62 (3H, d, $^2J_{HH}$ = 7.45 Hz, Ar*H*), 7.33–7.26 (6H, m, Ar*H*). MS calcd for $C_{27}H_{18}N_6$ *m*/*z* 426.16, found 427.16. Anal. Calcd. for $C_{27}H_{18}N_6$: C, 76.04; H, 4.25; N, 19.71. Found: C, 73.37; H, 4.91; N, 18.55.

2.3. Characterization

The samples were prepared in KBr pellet form for FTIR spectroscopy measurement. The spectra were recorded using a Thermo Nicolet Nexus 670 with 32 scans at a resolution of 2 cm^{-1}. A frequency range of 4000–400 cm^{-1} was observed using a deuterated triglycinesulfate (DTGS) detector. The temperature dependence FTIR spectra were collected using an in-house temperature-controller attachment.

^{1}H NMR spectra were verified on a Bruker Avance spectrometer (Germany) operating at Larmor frequencies of 500.13 MHz. For spin-lattice relaxation time measurements, an amount of each derivative containing 39.6 mM benzimidazole units was dissolved in DMSO-d_6. T_1 value was evaluated from inversion recovery ($\pi-\tau-\pi/2$) measurements at room temperature.

Single crystal structure analysis was carried out by a Rigaku R-axis Rapid-R X-ray diffractometer with graphite monochromated Mo Kα radiation at 296 K. The structure was determined by the direct method (SIR92) and refined by full-matrix least-squares on F^2 with a RAPID AUTO program. All non-hydrogen atoms were refined with anisotropic displacement parameters as well as the fractional coordinates. The single crystals were obtained from sublimation in an evacuated tube.

Thermal degradation profiles were investigated by a Perkin Elmer Pyris Diamond thermogravimetric/differential thermal analyzer from 30 to 800 °C at a heating rate of 10 °C per min under a N_2 atmosphere.

Wide-angle X-ray diffraction (WAXD) analysis was conducted by a simultaneous measurement system of a Rigaku X-ray powder diffractometer/RINTTTR III Thermo plus DSC with Cu Kα radiation.

Table 1
Crystal data and structure refinement parameters for **B-1** to **B-3**.

Compound	**B-1**	**B-2**	**B-3**
Empirical formula	$C_7H_6N_2$	$C_{16}H_{14}N_4$	$C_{20}H_{14}N_4$
Formula weight	118.14	262.31	310.36
Temperature (K)	296(1)	296(1)	296(1)
Wavelength (Å)	0.71075	0.71075	0.71075
Crystal system	Orthorhombic	Orthorhombic	Orthorhombic
Space group	*Pna*21	*Pbca*	*Pbca*
Unit cell dimensions			
a (Å)	13.5107(7)	8.4460(13)	10.266(3)
b (Å)	6.8158(3)	9.9346(14)	9.748(3)
c (Å)	6.9447(4)	15.307(2)	14.960(4)
V (Å^3)	639.51(6)	1284.4(3)	1497.2(8)
Z	4	4	4
D_{calc} (g cm^{-3})	1.227	1.356	1.377
μ (mm^{-1})	7.72	8.44	8.47
Maximum and minimum transmission	0.896 and 0.992	0.117 and 0.996	0.714 and 0.983
Crystal size (mm^3)	0.30 × 0.10 × 0.10	0.15 × 0.05 × 0.05	0.70 × 0.20 × 0.20
Reflections collected	5941	11,609	1582
Independent reflections	1462 [*R*(int) = 0.022]	1469 [*R*(int) = 0.240]	374 [*R*(int) = 0.097]
Observed reflections [$I > 1\sigma(I)$]	1209	419	5315
Goodness-of-fit on F^2	0.8	1.076	1.657
Final *R* indices [$I > 2\sigma(I)$]	R_1 = 0.0265	R_1 = 0.0370	R_1 = 0.0714
	ωR_2 = 0.052	ωR_2 = 0.0528	ωR_2 = 0.1372
Largest diffraction peak and hole deposition number (e Å^{-3})	0.17 and −0.32	0.14 and −0.19	1.16 and −2.19

The resistance was determined via complex impedance method using a μAUTOLAB Type III potentiostat/galvanostat in a frequency range of 500 kHz to 1 MHz and an a.c. signal amplitude of 50 mV. The sample was prepared by dropping the DMSO solution of each benzimidazole derivative (0.85 M benzimidazole unit, 20 μL) on glass filters and drying at 100 °C for 6 h. This procedure was repeated five times before drying under vacuum at 100 °C for 2 days. Two pieces of glass filter were gathered and doped with PPA (30 μL) before assembling in a sealed-off Teflon cell using copper as electrodes. The mole ratio of benzimidazole unit: PPA was 1:3.5. The conductivity (σ) was calculated from impedance data according to:

$$\sigma = \left(\frac{1}{R}\right)\left(\frac{L}{A}\right) \quad (1)$$

where: *L* is the sample thickness; *A* is the cross-sectional area between membrane and electrode (0.4418 cm^2); *R* is the resistance derived from the intersection of Nyquist plot on the real axis at the imaginary part equal to zero.

3. Results and discussion

3.1. Structural characterization

The synthesis routes of the model compounds are based on the nucleophilic substitution of an excess amount of diamine to acid chloride derivatives. The spectroscopic data of **B-2** and **B-4** have been described in the previous work [17]. In this study, **B-3** was prepared via amidation of terephthaloyl chloride and 1,2-phenylenediamine. The FTIR spectrum confirmed the structure of **B-3** from the characteristic peaks at 3400–2500 cm^{-1} (hydrogen bonded N–H stretching of benzimidazole unit), 1622 cm^{-1} (C=N stretching), 1453 cm^{-1} (C=C stretching), and 738 cm^{-1} (C–H bending of aromatic ring). The ^{1}H NMR spectrum indicated the chemical shifts of **B-3**, i.e., at 8.36 ppm (protons of the benzene ring), 7.71, 7.57 and 7.26 ppm (protons of aromatic ring in benzimidazole), and 13.03 ppm (N–H proton). In addition, the MALDI-TOF spectrum confirmed the successful preparation of **B-3** from the parent peak at m/z = 310.64 which is equal to the molecular weight of **B-3** (formula weight of **B-3** is 310.12). The CHN analysis result also supports the structure of **B-3** (see detailed synthesis and structural characterization in S1–S4).

3.2. Investigation of hydrogen bond network and molecular structure assembly

3.2.1. Single crystal structure

X-ray single crystal structure analysis was applied to determine an exact molecular structure including its bonding distance, molecular orientation, and the possible hydrogen bond network. The crystallographic data and parameters are summarized in Table 1. The crystal structure of **B-1** has been reported in the past [17,20]. In this work, the single crystal of **B-1** was prepared by sublimation and it was found that the crystal structure of the compound was a orthorhombic crystal system with $Pna2_1$ space group (Fig. 1(a)). The result is similar to that reported by Vijayan et al. [20] although their objective was different. Here, single crystals of **B-2** and **B-3** were successfully prepared by sublimation technique. The crystal structure of **B-3** is similar to that of the report by Bei et al. [19]. Both **B-2** and **B-3** are in orthorhombic system with *Pbca* space group (Fig. 1(b) and Fig. 1(c)). As the hydrogen bond network is directly related to proton transfer [10], the H-bond networks of the model compounds were intensively studied in terms of the packing structure. The packing structures revealed the hydrogen bond (NH···N) formation among the adjacent benzimidazole molecules with varied hydrogen bond distances of 2.85 Å for **B-1** and **B-2**, and 3.02 Å for **B-3**. Considering the hydrogen bond network channel, the significant differences of hydrogen bond patterns detailed by single crystal structure analyses were determined, as illustrated in Fig. 2. It is clear that both mono- and difunctional benzimidazoles form hydrogen bond chains in a lamellar structure. The structure is relevant to that reported by Yamada and Honma [15]. However, the patterns of the hydrogen bond formation are significantly different. Monofunctional benzimidazole forms two directions of hydrogen bond chains with mutually perpendicular orientation in the *bc*-plane (Fig. 2(a)) whereas difunctional benzimidazole, **B-2** and **B-3**, shows the parallel H-bond chains along *b*-axis in all the layers (Fig. 2(b) and (c)). For **B-4**, trifunctional benzimidazole, preliminary structural analysis [21] confirmed that the hydrogen bonds are among neighbouring benzimidazole rings along the c axis generating the helical hydrogen bond chains in the columnar structure as demonstrated in Fig. 2(d). The detailed structure analysis will be reported elsewhere.

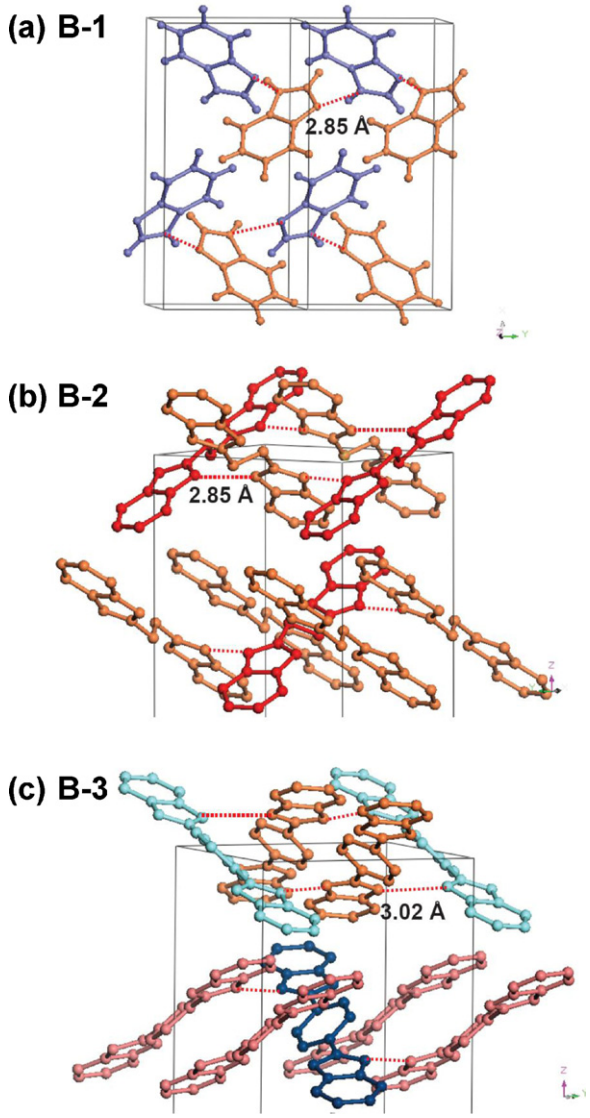

Fig. 1. X-ray crystal packing structure diagrams of (a) **B-1**; (b) **B-2**; and (c) **B-3** with hydrogen bond interaction. Figures built with Materials Studio (Accelrys, Inc.) software.

3.2.2. *Information of molecular assembly based on proton spin-lattice relaxation time*

The movement of protons is largely dependent on the molecular assembly. This can be traced using the proton spin-lattice relaxation time (T_1). Because the N–H proton plays an important role in proton transfer, T_1 values of the protons in **B-1**, **B-2**, **B-3**, and **B-4** at the chemical shifts of 12.41, 12.31, 13.03 and 13.37 ppm, respectively, are comparatively analyzed (Fig. 3). As T_1 strongly depends on several factors, especially the concentrations, the type of solvent and the temperature [22–24], the samples at a certain concentration of benzimidazole moieties in DMSO-d_6 were prepared and the T_1 measurements were carried out at 25 °C.

In general, a proton with the longer T_1 indicates less restricted mobility [25], in other words, that particular proton is under an atmosphere with more space for free movement. In the case of **B-1**, T_1 of N–H is extremely long compared with the others. It is clear that an increase in the number of benzimidazole units greatly reduces the T_1 value. Although T_1 represents the proton mobility among benzimidazole derivatives in solution, the result implies how the hydrogen bond network induces the tighter packing structure of **B-4** compared with that of **B-3**, **B-2**, or **B-1**.

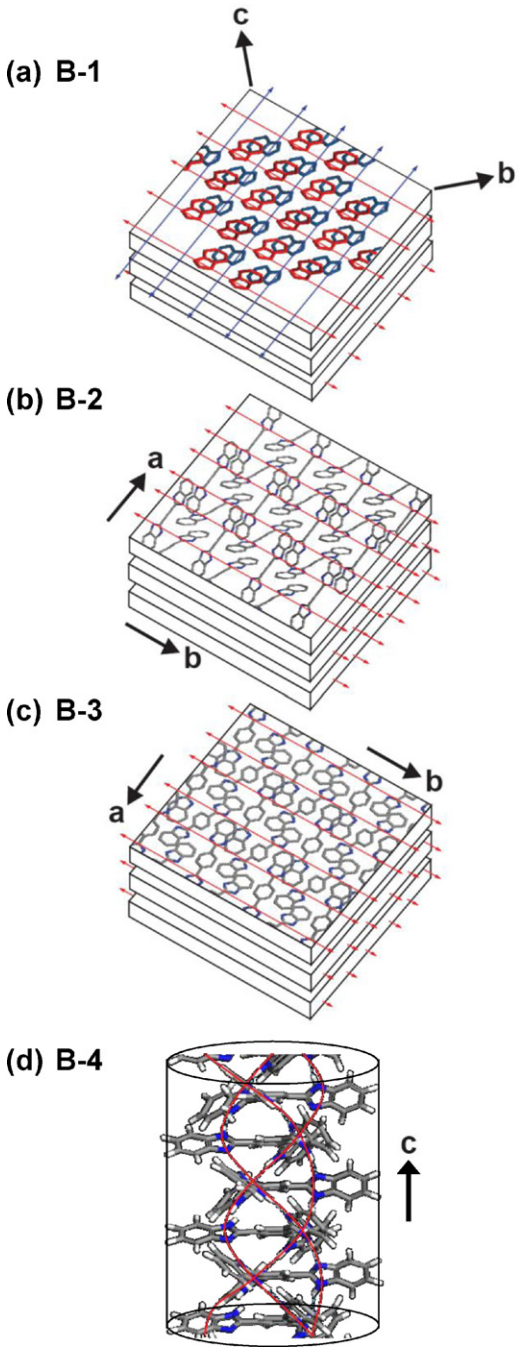

Fig. 2. Schematic draws of perpendicular hydrogen bond chains of (a) **B-1**, the parallel hydrogen bond chains of (b) **B-2** and (c) **B-3** formed in lamellar structures and helical hydrogen bonds chains formed in columnar structure of (d) **B-4**. Some hydrogen atoms are excluded to clarify viewing.

3.2.3. *Thermal degradation behaviours of benzimidazole-based compounds*

The thermal stability of the model compounds was studied by thermogravimetric (TGA) analysis. All compounds demonstrated good thermal stability up to 200 °C, therefore they were appropriate for the use in an intermediate temperature PEMFC. Monofunctional benzimidazole, **B-1**, shows the lowest degradation temperature (T_d), whereas di- and trifunctional benzimidazoles have higher degradation temperatures (~400 to 500 °C) (Fig. 4). It should be noted that in the case of difunctional molecules with differently connected structures, the benzene-linked structure (**B-3**) shows a higher T_d than an ethylene-linked structure (**B-2**). Combining T_d

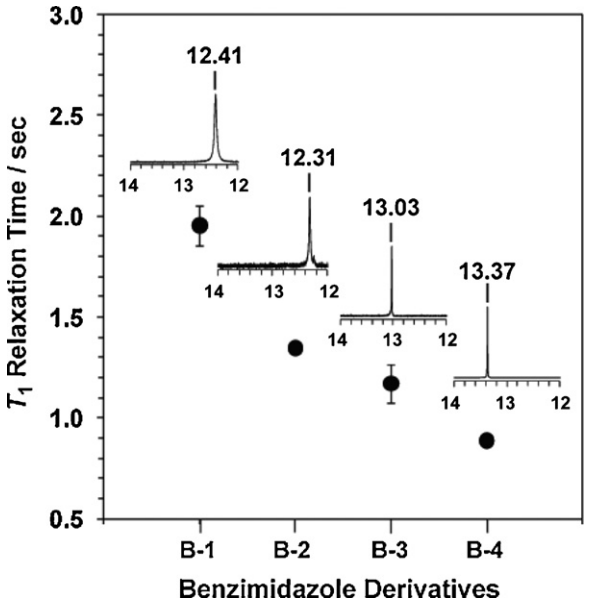

Fig. 3. T_1 relaxation times of **B-1**, **B-2**, **B-3**, and **B-4**.

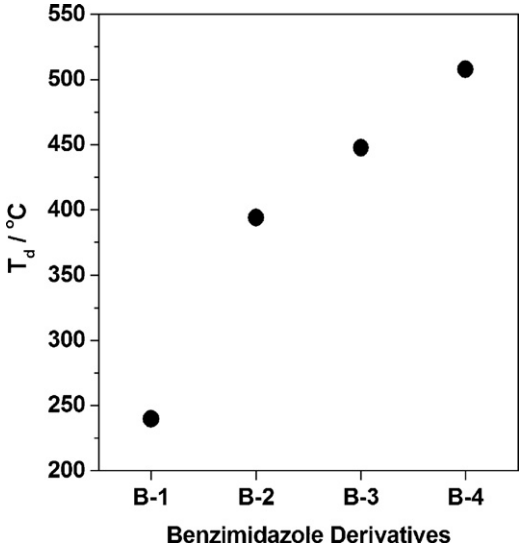

Fig. 4. Degradation temperatures of **B-1**, **B-2**, **B-3**, and **B-4**.

with the T_1 relaxation time, it is clear that the tight packing of the molecules leads to higher thermal stability in the order: **B-4** > **B-3** > **B-2** > **B-1**.

3.3. Investigation of proton transfer efficiency

3.3.1. Proton conductivity

Initially, the pellets of the model compounds were prepared by compressing the samples at 1.9×10^3 MPa. It was found that the conductivities of all derivatives were unstable and very low. Therefore, the compounds were doped thoroughly with PPA to immobilize the proton source, and the proton conductivity was measured as a function of temperature. The data in Fig. 5 shows that the conductivity of the PPA system increases gradually with an increase of temperature. A significant decrease of proton conductivity under PPA matrices is observed in the cases of **B-1**, **B-2**, and **B-3** doped with PPA. In the case of **B-4**/PPA, its conductivity is similar to PPA. The lowering of proton conductivity indicates the role of PPA as a strong protonic source for proton hopping through

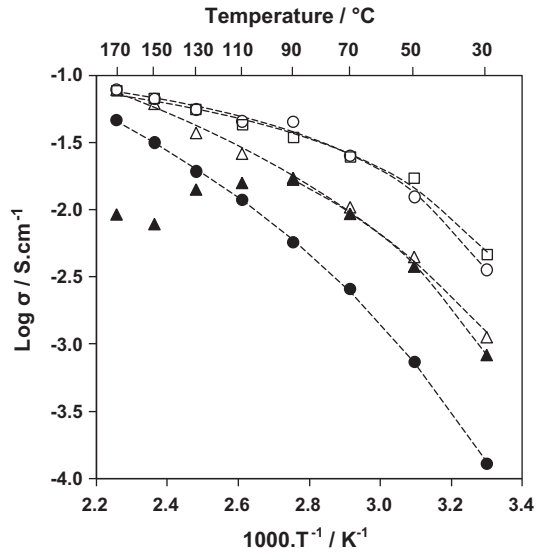

Fig. 5. Arrhenius plot comparing experimental data of PPA (□); **B-1**/PPA (●); **B-2**/PPA (△); **B-3**/PPA (▲); **B-4**/PPA (○) with value obtained from VTF equation fitting (broken lines).

heterocycles [13,26]. Considering the hydrogen bond network of **B-4**, it is possible that the columnar packing allows efficient proton transfer (more discussion in Section 3.3.2) and thereby results in the higher conductivity of **B-4** compared with that of **B-1**, **B-2** or **B-3**.

Fig. 5 also shows that the conductivities of benzimidazole derivatives doped with PPA increase with temperature. The PPA doping level was controlled to be equal for all derivatives so that their conductivities could be directly compared. The conductivity order of **B-4** > **B-2** and **B-3** > **B-1** shows how each packing structure offers an efficient proton transfer route. Unexpectedly, the conductivity of **B-3** is lower than that of other compounds after 110 °C. The fact that the structure of **B-3** represents a rigid molecule, i.e., benzene-linked benzimidazoles, it can be suspected that the proton transfer may be limited due to difficulty in the molecular movement of **B-3** (see more discussion in Sections 3.4 and 3.5).

3.3.2. Activation energy for proton transfer

Two main possible proton transfer mechanisms contribute to the proton conductivity in phosphoric acid-doped systems, namely, the structural diffusion (Grotthuss mechanism) and the vehicle mechanisms have been proposed [27–29]. The good agreement of the conductivity–temperature relationship with Arrhenius behaviour (Eq. (2)) suggests that the proton transfer proceeds via a Grotthuss mechanism in which protons transport through phosphate ions of $H_4PO_4^+$ and $H_2PO_4^-$ as can be analyzed as follows:

$$\log \quad \sigma = \log \quad \sigma_o - \left(\frac{E_a}{RT}\right) \tag{2}$$

where: σ is proton conductivity (S cm^{-1}); σ_o is pre-exponential factor (J mol^{-1}); E_a is activation energy for proton conduction (J mol^{-1}); R is gas constant (8.314 J K^{-1} mol^{-1}); and T is the absolute temperature (K).

By contrast, the deviation from Arrhenius behaviour which can be explained by the Vogel–Tamman–Fulcher (VTF) equation (Eq. (3)), indicates proton transfer through the material based on neutral or charged vehicles.

$$\log \quad \sigma = \log \quad \sigma_o - \left(\frac{E_a}{R(T - T_0)}\right) \tag{3}$$

where T_0 is the Vogel temperature.

Table 2
VFT parameters obtained from fitting the proton conductivity data to Eq. (3).

Sample	Doping ratio per mole benzimidazole	E_a (kJ mol^{-1})	T_0 (K)	σ_0	R^2
PPA		0.58	258	0.17	0.9984
B-1/PPA	3.5	3.27	210	2.19	0.9997
B-2/PPA	3.5	2.30	210	1.14	0.9978
B-3/PPA	3.5	1.05 (in the temperature range 30–90 °C)	250	0.65	0.9998
B-4/PPA	3.5	0.55	264	0.18	0.9985

In the intermediate temperature range (100–150 °C), the linear relationship of the Arrhenius plots of PPA, **B-1**/PPA, **B-2**/PPA, and **B-4**/PPA indicates that the Grotthuss mechanism is dominant. A divergence from the linear line, however, is observed in the low temperature range (30–90 °C). To determine the activation energy of proton transfer which covers entire temperature range, the data were found to be better fitted with the VTF equation (broken lines in Fig. 5) as seen from the VTF parameters summarized in Table 2. In the case of **B-3**/PPA, although the conductivity data could not be fitted with the VTF equation in the intermediate temperature range the segment in the range of 30–90 °C was well fitted.

As the boiling point of PPA is as high as 300 °C, PPA maintains its stability on glass filters to support the proton transfer in the heterocyclic compounds even the proton conductivity measurement was carried out at the temperature above 100 °C. PPA shows an activation energy (E_a) as low as 0.58 kJ mol^{-1}, while the derivatives show E_a values in the range of 0.55–3.27 kJ mol^{-1}. This reflects how PPA helps in the proton transfer. **B-4** doped with PPA shows the lowest activation energy (0.55 kJ mol^{-1}) which is as low as that of PPA. This suggests that the structure of **B-4** provides an effective proton transfer pathway and at the same time the doping agent of PPA initiates the proton transfer. Here, it is found that the greater the number of benzimidazoles in a single molecule, the lower the E_a, and, as a result, the higher the proton conductivity.

3.4. Investigation of hydrogen bond network and molecular packing structure under variable temperatures

3.4.1. Hydrogen bond network under temperature dependence FTIR studies

Temperature dependence FTIR is a good tool to follow how the molecular interaction changed under the variation of temperatures. As benzimidazole shows a broad absorption N–H stretching in the region of 3400–2500 cm^{-1}, the changes of this absorption band with the temperature were focused.

When the samples were heated from room temperature to 200 °C, the FTIR spectra were gradually shifted toward a higher wavenumber (Fig. 6(a)). The shifts of FTIR spectra are also similar to those reported previously [17]. This implies a weakening of the hydrogen bonds on raising the temperature.

It is important to note that the shift of the broad hydrogen bond N–H group to the higher wavenumber with an increase in temperature results in a particular isobestic position. For example, in the case of **B-4**, the isobestic position at 2802 cm^{-1} is the position that shows a decrease of the strong hydrogen bond N–H in the benzimidazole functional group at below this point and an increase in the weak hydrogen bond N–H above this point during heating (Fig. 6a (iv)). Isobestic points are found at 2933 cm^{-1} for **B-2** (Fig. 6a (ii)), at 3025 cm^{-1} for **B-1** (Fig. 6a (i)), and at 3144 cm^{-1} for **B-3** (Fig. 6a (iii)), respectively.

The fact that the position of the broad peaks with the isobestic point of the hydrogen bond reflects the level of energy required to allow the resonance structure of the imidazole ring and a change from covalent bond to hydrogen bond (Fig. 6(b)). Comparison of the peak position, especially the isobestic point, gives the order of hydrogen bond strength. In other words, the lower wavenumber, the less is the energy required for changing a covalent bond N–H to a hydrogen bond N···H, and as a result the more favourable allow proton transfer. Based on the comparison of isobestic positions (Fig. 6(c)), the energy level to change the N–H of benzimidazole to an intermolecular hydrogen bond is in the order: **B-1** > **B-2** > **B-4**. In other words, the ease of proton transfer is in the order: **B-4** > **B-2** > **B-1**.

Combining the results with that of T_1, the role of hydrogen bond can be summarized as follows. **B-4** shows the lowest T_1 value suggesting the most crowded atmosphere to obstruct the free movement of proton through space as compared with the others (Fig. 3). In other words, **B-4** might be an assembly in a hydrogen bond network and this pre-forms the packing structure which favours a change from strong hydrogen bond to weak hydrogen bond resulting in requiring less energy than **B-1** and **B-2**.

In the case of **B-3**, the result is different from the others. It should be noted that **B-3** hardly maintains its hydrogen bond compared with other compounds during thermal treatment; but it shows a relatively tight packing as studied by T_1 relaxation time (Fig. 3) and T_d (Fig. 4). This might be due to the fact that the packing structure is not only based on the hydrogen bond but also the π–π interaction [30].

3.4.2. Molecular packing structure under temperature dependence WAXD

The temperature dependence WAXD was verified to see how the hydrogen bond is related to the packing structure under a temperature variation ranging from 25 to 200 °C. The WAXD profiles of the model compounds as a function with temperature are shown in Fig. 7. The WAXD patterns of **B-1** (Fig. 7(a)) illustrate the significant peak shifts (13.03°, 14.59°, 18.31°, 19.41°, 22.56°, 23.61°, 26.33°, 26.96° and 28.83°) to lower angles during heat treatment. The crystalline phase disappears after the temperature reaches the melting point (171 °C). In addition, a crystalline peak does not exist during cooling the temperature down. This implies that the packing structure of **B-1** is unstable when subjected to a temperature variation. In the case of **B-3** (Fig. 7(c)), the peaks at 11.78°, 14.60°, 17.21°, 19.13°, 21.71°, 23.70° and 25.25° 2θ shift to lower angles and back to the original position during heating–cooling process. This suggests a reversible thermal expansion–contraction packing structure of **B-3**. This phenomenon is also observed with **B-2** (Fig. 7(b)). For **B-4**, the peak shifts are only slight (Fig. 7(d)) and this indicates a stable packing structure without any changes over the temperature range 25–200 °C [17]. Additionally, the sharp diffraction patterns of all molecules during increasing temperature show that a high-ordered structure is maintained in each derivative even the temperature is as high as 170 °C.

3.5. Preferable molecular structure and hydrogen bond network for enhancing proton conductivity

It is now necessary to investigate how the number of benzimidazole units, mono-, di- and trifunctional is related to the proton conductivity. Based on the systematic variation of the number of benzimidazoles, the factors involved in proton transfer efficiency

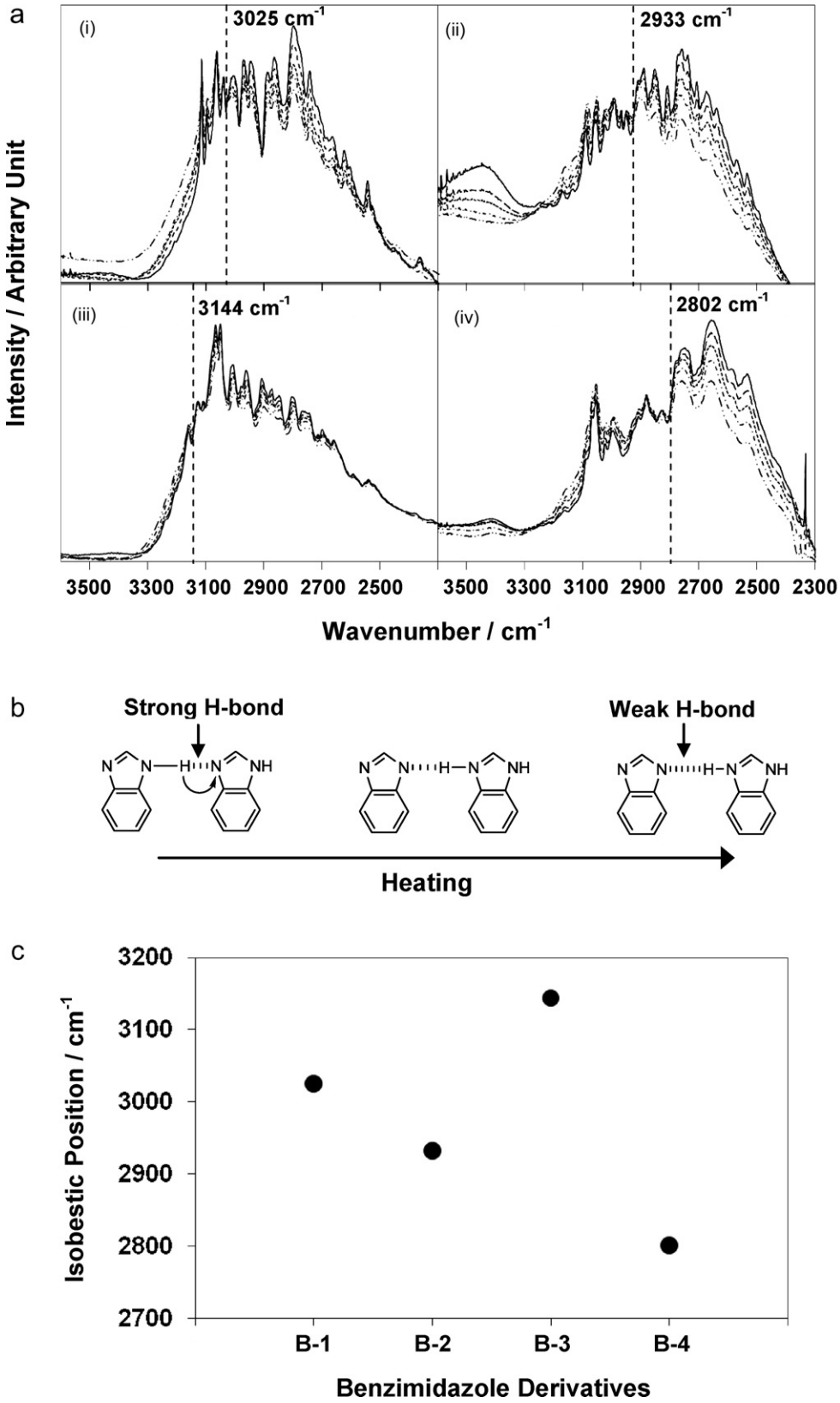

Fig. 6. (a) Temperature dependence FTIR spectra of (i) **B-1**; (ii) **B-2**; (iii) **B-3**; and (iv) **B-4** at room temperature (——), 60 °C (- - -), 100 °C (· · ·), 140 °C (·–·–·–) and 200 °C (–··–··); (b) hydrogen bond possibly changing from strong to weak during heating; and (c) isobestic positions of **B-1**, **B-2**, **B-3**, and **B-4**.

are, therefore, not only the hydrogen bond but also the molecular packing structure and/or molecular assembly. On the assumption that the proton conductivity will be higher with a more densely packed structure and a stronger hydrogen bond network, the discussions are as follows. The study of T_1 and T_d combined with temperature dependence WAXD suggests that the molecular packing structure is in the order of: **B-1** < **B-2** < **B-3** < **B-4**. This results in the proton conductivity in the order: **B-4** > **B-2** > **B-1**. In the case of

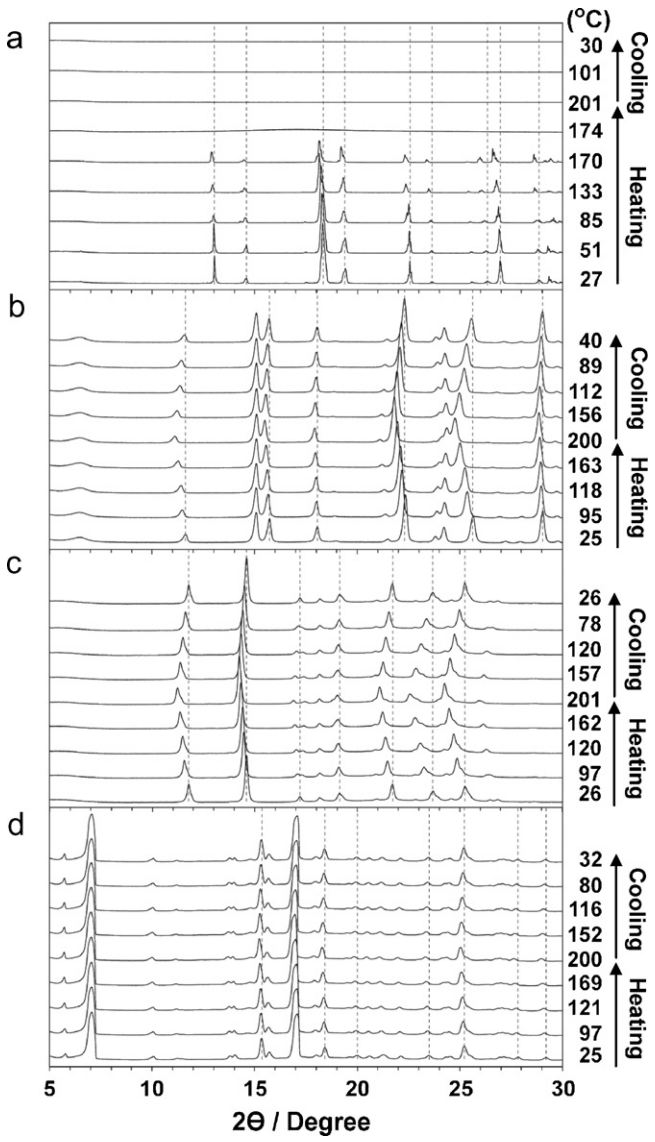

Fig. 7. WAXD patterns of (a) **B-1**; (b) **B-2**; (c) **B-3**; (d) **B-4** during heating and cooling at 3 °C per min under N_2 atmosphere.

B-3, although the hydrogen bond network pattern is similar to that of **B-2**, the fact that it contains a benzene ring means that the stacking conformation might also restrict the molecular movement and favour the proton transfer.

It is important to note that the hydrogen bond formation of **B-4** leads to a helical packing as confirmed by single crystal analysis. Based on this structure, it is possible that the protons can move along the long columnar axis through the NH···N hydrogen bonds created between the neighbouring benzimidazole rings. Although this speculative mechanism of proton transfer needs further clarification, this plausible image explains why the trifunctional benzimidazole shows the most significant proton conductivity compared with the other compounds.

The proton transfer for benzimidazoles can be discussed as follows. It is found that when the temperature is higher, the conductivities of the derivatives become closer to each other. Initially, the protonation of benzimidazole accelerates the proton transfer through the hydrogen bond, as mentioned above. A larger number of benzimidazoles and a more tightly packed structure are more preferable conditions for proton transfer. When the temperature is increased further, the hydrogen bond becomes weaker and at the same time the molecular motion becomes significant. At a temperature as high as 170 °C, it is possible that the proton transfer may also arise from the movement of PPA molecules along the benzimidazole network.

4. Conclusions

The present work shows: (i) how benzimidazoles develop hydrogen bond patterns and their consequent packing structure; (ii) how hydrogen bond, as well as the packing structure, play a role in proton transfer in terms of proton conductivity. A series of model compounds containing one to three benzimidazole units reveals that the benzimidazoles form hydrogen bond networks of which one and two benzimidazoles are assemble in lamellar structure, whereas the three benzimidazoles are in columnar arrangement. Proton conductivity increases significantly with temperature when the benzimidazoles are aligned in the manner that the hydrogen bond between benzimidazoles effectively form. At that time, the transfer of protons from one benzimidazole unit to another is possible. If the benzimidazoles form a columnar packing, the proton transfer is much more efficient, as seen in the case by **B-4**. In contrast, even the proton transfer through the hydrogen bond network of benzimidazoles is possible, but if the benzimidazoles are under other molecular interaction, such as π–π interaction to obstruct the molecular mobility, the proton transfer becomes less as seen for **B-3**.

Acknowledgements

The authors acknowledge the National Research University Project of the Commission of Higher Education and the Ratchadaphiseksomphot Endowment Fund, Chulalongkorn University (EN276B). One of the authors (A.P.) is grateful for a Ph.D. scholarship from the Development and Promotion of Science and Technology Talents Project (DPST), Thailand and Japan Student Services Organization (JASSO), Japan.

Appendix A. Supplementary data

Supplementary data associated with this article can be found, in the online version, at doi:10.1016/j.jpowsour.2011.02.093.

References

[1] A.V. Anantaraman, C.L. Gardner, J. Electroanal. Chem. 414 (1996) 115–120.
[2] K.A. Mauritz, R.B. Moore, Chem. Rev. 104 (2004) 4535–4585.
[3] M.A. Hickner, H. Ghassemi, Y.S. Kim, B.R. Einsla, J.E. McGrath, Chem. Rev. 104 (2004) 4587–4612.
[4] S.U. Jeong, E.A. Cho, H.-J. Kim, T.-H. Lim, I.-H. Oh, S.H. Kim, J. Power Sources 158 (2006) 348–353.
[5] M. Rikukawa, K. Sanui, Prog. Polym. Sci. 25 (2000) 1463–1502.
[6] Q. Li, R.H. He, J.O. Jensen, N.J. Bjerrum, Chem. Mater. 15 (2003) 4896–4915.
[7] R. Gosalawit, S. Chirachanchai, H. Manuspiya, E. Traversa, Catal. Today 118 (2006) 259–265.
[8] C. Yang, P. Costamagna, S. Srinivasan, J. Benziger, A.B. Bocarsly, J. Power Sources 103 (2001) 1–9.
[9] J. Zhang, Z. Xie, J. Zhang, Y. Tang, C. Song, T. Navessin, Z. Shi, D. Song, H. Wang, D.P. Wilkinson, Z.-S. Liu, S. Holdcroft, J. Power Sources 160 (2006) 872–891.
[10] W. Munch, K.D. Kreuer, W. Silvestri, J. Maier, G. Seifert, Solid State Ionics 145 (2001) 437–443.
[11] K.D. Kreuer, A. Fuchs, M. Ise, M. Spaeth, J. Maier, Electrochim. Acta 43 (1998) 1281–1288.
[12] U. Sen, S.Ü. Çelik, A. Ata, A. Bozkurt, Int. J. Hydrogen Energy 33 (2008) 2808–2815.
[13] M. Schuster, W.H. Meyer, G. Wegner, H.G. Herz, M. Ise, M. Schuster, K.D. Kreuer, J. Maier, Solid State Ionics 145 (2001) 85–92.
[14] A. Bozkurt, W.H. Meyer, G. Wegner, J. Power Sources 123 (2003) 126–131.
[15] M. Yamada, I. Honma, J. Phys. Chem. B 108 (2004) 5522–5526.
[16] M. Yamada, I. Honma, Polymer 46 (2005) 2986–2992.
[17] P. Totsatitpaisan, K. Tashiro, S. Chirachanchai, J. Phys. Chem. A 112 (2008) 10348–10358.

[18] X.-P. Li, J.-Y. Zhang, M. Pan, S.R. Zheng, Y. Liu, C.Y. Su, Inorg. Chem. 46 (2007) 4617–4625.
[19] F. Bei, F. Jian, X. Yang, L. Lu, X. Wang, S.S.S. Raj, H.-K. Fun, Acta Crystallogr., Sect. C: Cryst. Struct. Commun. 56 (2000) 718–719.
[20] N. Vijayan, N. Balamurugan, R.R. Babu, R. Gopalakrishnan, P. Ramasamy, W.T.A. Harrison, J. Cryst. Growth 267 (2004) 218–222.
[21] K. Tashiro, A. Pangon, H. Hasegawa, M. Yamazaki, P. Totsatitpaisan, S. Chirachanchai, Polym. Prepr. Jpn. 58 (2009) 5702–5703.
[22] J. Frahm, J. Phys. Chem. 84 (1980) 1393–1400.
[23] J.J. Fontanella, C.A. Edmondson, M.C. Wintersgill, Y. Wu, S.G. Greenbaum, Macromolecules 29 (1996) 4944–4951.
[24] H. Ye, J. Huang, J.J. Xu, N.K.A.C. Kodiweera, J.R.P. Jayakody, S.G. Greenbaum, J. Power Sources 178 (2008) 651–660.
[25] E.H. Sanders, K.A. McGrady, G.E. Wnek, C.A. Edmondson, J.M. Mueller, J.J. Fontanella, S. Suarez, S.G. Greenbaum, J. Power Sources 129 (2004) 55–61.
[26] S. Feng, Y. Shang, S. Wang, X. Xie, Y. Wang, Y. Wang, J. Xu, J. Membr. Sci. 346 (2010) 105–112.
[27] S.Ü. Çelik, A. Bozkurt, Eur. Polym. J. 44 (2008) 213–218.
[28] S.Ü. Çelik, A. Aslan, A. Bozkurt, Solid State Ionics 179 (2008) 683–688.
[29] A. Aslan, A. Bozkurt, Langmuir 26 (2010) 13655–13661.
[30] R. Boča, A. Boča, L. Dlháň, K. Falk, H. Fuess, W. Haase, R. Jaroščiak, B. Papánková, F. Renz, M. Vrbová, R. Werner, Inorg. Chem. 40 (2001) 3025–3033.